Geophysical Journal International

Geophys. J. Int. (2015) **201,** 53–60 doi: 10.1093/gji/ggu498

GJI Marine geosciences and applied geophysics

Efficient full-waveform inversion with normalized plane-wave data

Taekhyun Kwon, Soon Jee Seol and Joongmoo Byun

Department of Natural Resources and Geoenvironmental Engineering, Hanyang Univ., 222 Wangsimni-Ro, Seongdong-gu, Seoul 133-791, *Korea.*
E-mail: ssjdoolly@hanyang.ac.kr

Accepted 2014 December 31. Received 2014 December 31; in original form 2014 August 29

SUMMARY

Full-waveform inversion (FWI) provides a high-resolution velocity model, but carries a high computational cost. Additionally, modern seismic acquisition, with dense sources and receivers, generates massive data, resulting in an even greater computational cost. To reduce the computational burden of FWI, we have developed an FWI algorithm using plane-wave data. Using this approach, plane-wave gathers transformed from shot gathers are used as input data in inversion. Because the number of plane-wave gathers is generally far smaller than that of common shot gathers for the same data set, we can significantly reduce the computational cost and efficiently handle a massive data set. 2-D numerical testing showed that the developed FWI algorithm was more efficient than conventional FWI using common shot gathers. However, estimation of the source wavelet is essential for successful FWI in most cases. The developed FWI algorithm here excludes the source effect by using the normalized wave field instead of estimating the source wavelet through inversion processing. When the FWI algorithm was applied to data generated by slightly different source wavelets, a good velocity model was reconstructed without any artefacts from the effects of the different source wavelets. Furthermore, it presented a stable inversion result with only small artefacts, even though we used random noise-added data. Finally, in a numerical experiment with data from the SEG/EAGE 3-D overthrust model, which includes complex structures and thin layers, the developed FWI algorithm yielded a reasonable reconstructed velocity model.

Key words: Inverse theory; Seismic tomography; Computational seismology; Wave scattering and diffraction; Wave propagation; Acoustic properties.

INTRODUCTION

Due to advances in computer science, the full-waveform inversion (FWI) technique has been improved by many researchers over the past two decades (Pratt *et al.* 1998; Pratt 1999; Shin & Min 2006; Operto *et al.* 2007). However, because more sources and receivers are used in modern seismic acquisition, FWI still carries a great computational cost, especially in the case of massive 3-D data composed of thousands of shot gathers. The migration technique also has a computational cost problem. To effectively reduce the computational burden, Romero *et al.* (2000) introduced the simultaneous source method using the concept of phase-encoded shot gathers for pre-stack depth migration (PSDM). They tested various encoding methods, and among those, random phase encoding worked best. After its effectiveness was demonstrated for PSDM, the simultaneous source method was employed by several researchers used using random phase encoding to perform FWI with fixed-spread data, such as land and ocean bottom cable acquisitions (Krebs *et al.* 2009; Boonyasiriwat & Schuster 2010; Ben-Hadj-Ali *et al.* 2011; Guitton & Díaz 2012). The key to this approach was that crosstalk artefacts due to simultaneous sources can be suppressed by stacking the super shots, which are constructed by summing distributed individual shots. However, the efficiency and accuracy of the encoding technique were dependent on the choice of the random shots or the number of encoded sources in a super shot, and this method can be more sensitive to random noise in the data, depending on the source assembling method (Ben-Hadj-Ali *et al.* 2011).

An alternative strategy for reducing computational cost is to transform the recorded shot gathers to plane-wave gathers with different ray parameters. This plane-wave method avoids the disadvantages of random phase encoding; unlike the random phase encoding approach, the plane-wave method is not sensitive to random noise and can be easily applied to marine geometry (Liu *et al.* 2006; Tao & Sen 2013). Because this approach uses far fewer ray parameters than the number of shots in modelling and inversion, the data can be reduced considerably.

The plane-wave method was first applied to the migration scheme (Whitmore 1995; Zhang *et al.* 2005; Liu *et al.* 2006; Stoffa *et al.* 2006; Dai & Schuster 2013). Zhang *et al.* (2005) suggested how many ray parameters should be used to successfully apply the plane-wave method and improve the efficiency of waveequation migration. Liu *et al.* (2006) mathematically proved the equivalence of shot

and plane-wave migration and showed that cross talk artefacts are suppressed reasonably well by using a sufficient number of ray parameters in 3-D plane-wave migration. If we transform seismic data to plane-wave data without sufficient spatial sampling and aperture, artefacts can be generated in data space. However, the requirement for sufficient spatial sampling and aperture is commonly satisfied in modern seismic acquisitions, so the plane-wave approach can be used widely.

Vigh & Starr (2008) used the plane-wave approach in time domain FWI and showed that using plane-wave gathers can dramatically reduce the number of computations. Tao & Sen (2013) reported that the plane-wave gather could be realized by a phase shift in the frequency domain, and developed a 2-D frequency-domain FWI algorithm with plane-wave data. Additionally, they analysed the effect of the selection of ray parameters on the inversion.

In this study, we developed an efficient frequency-domain 3-D FWI algorithm using plane-wave encoding. It included finite element modelling and used the normalized wavefield technique to remove the source effect. To verify the efficiency and accuracy of the developed FWI, we compared its result with that from the conventional FWI, which was applied to individual common-shot gathers. Additionally, the normalization wavefield technique was tested, and the effect of random noise on the algorithm was investigated. To show its imaging capability for 3-D data, we applied our FWI to the data from the 3-D SEG/EAGE overthrust model.

PLANE-WAVE GATHERS IN THE TIME DOMAIN

Time-domain shot gathers are usually obtained from seismic data acquisition. To carry out FWI with plane-wave data, we needed to transform shot gathers into plane-wave gathers. Fig. 1 represents a schematic diagram of plane-wave construction in the time domain by time delay. Time domain plane-wave gathers are composed by a linear slant stack operating on common receiver gathers followed by a time delay, which is determined by the offset and ray parameter (Fig. 2). The time delay that is applied at each shot location, x_i, is defined as follows:

$$\Delta t_i(p) = p(x_i - x_0), \tag{1}$$

where $i = 1, 2, \ldots, N_x$, p is the ray parameter and x_0 is the plane-wave origin. In 3-D case, a linear slant stack operator is applied to not only x-direction but also y-direction. Therefore, eq. (1) is changed as follows:

$$\Delta t_{ij}(\mathbf{p}) = p_x(x_i - x_0) + p_y(y_j - y_0), \tag{2}$$

where $j = 1, 2, \ldots, N_y$, $\mathbf{p} = (p_x, p_y)$ is the ray parameter vector and (x_0, y_0) is the plane-wave origin. Fig. 3 represents 3-D plane-wave gathers for various p_x and p_y. As a linear slant stack operator on common receiver gathers is used not only to transfer data but also to

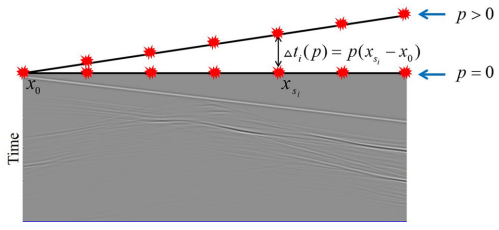

Figure 1. Schematic of plane wave in the time domain by time delay, depending on the source location and the ray parameter p (reproduced from Zhang *et al.* 2005).

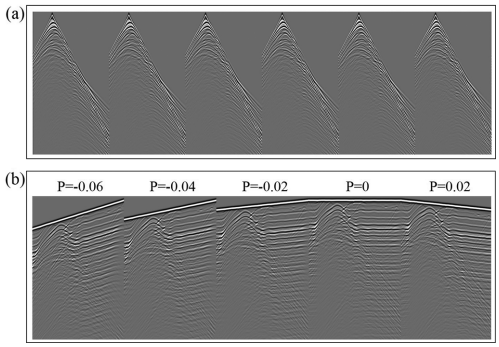

Figure 2. The time domain (a) shot gathers of recorded data and (b) plane-wave gathers transformed from shot gathers ($p = -0.06$ to 0.02 s km^{-1}).

improve the signal-to-noise ratio through the stacking process, the FWI with plane-wave data is robust compared with the conventional FWI for random noise.

The transformed plane-wave gathers were used as input data in our FWI. Thus, the number of observed traces used in inversion is not the number of shots (Ns) $\times$ the number of receivers (Nr) but the number of ray parameters (Np) $\times$ the number of receivers (Nr) (Table 1). Because Np is usually much smaller than Ns, we can reduce the computational cost by the amount of reduction in the data. The elapse time of the inversion should include the time required for transforming the shot domain data to the plane-wave domain data. However, this transformation is performed only once in the whole process and it takes a little time compared with entire time.

PLANE-WAVE GATHERS IN THE FREQUENCY DOMAIN

The conventional acoustic wave equation for a point source using a finite element method in the frequency domain can be written as (Marfurt 1984)

$$\mathbf{Ku}(\mathbf{x}, \omega) - \omega^2\,\mathbf{Mu}(\mathbf{x}, \omega) = \mathbf{f}(\omega)\delta(\mathbf{x} - \mathbf{x_s}), \tag{3}$$

where $\mathbf{K}$ is the stiffness matrix, $\mathbf{M}$ is the mass matrix, $\mathbf{u}$ is a displacement vector, $\mathbf{f}$ is the source vector and ω is the angular frequency. Eq. (3) can also be written as

$$\mathbf{S}(\mathbf{x}, \omega)\,\mathbf{u}(\mathbf{x}, \omega) = \mathbf{f}(\omega)\delta(\mathbf{x} - \mathbf{x_s}), \tag{4}$$

where the impedance matrix is given by $\mathbf{S} = \mathbf{K} - \omega^2\mathbf{M}$.

Physically, plane-wave gathers are the data received by a plane source with a different inclination accorded as a ray parameter, generated by using all sources simultaneously. Thus, the source term in eq. (4) has to be changed to construct the acoustic wave equation for the plane wave. Given that the time delay from eq. (1) corresponds to a phase shift in the frequency domain, forward modelling with the plane-wave source in the frequency domain can be written as (Tao & Sen 2013)

$$\mathbf{S}(\mathbf{x}, \omega)\mathbf{u}(\mathbf{x}, \mathbf{p}, \omega) = \sum_{x_s} \varphi(\mathbf{x}, \mathbf{x_s}, \mathbf{p}, \omega) f(\omega)\delta(\mathbf{x} - \mathbf{x_s}), \tag{5}$$

with the ith component of $\varphi(\mathbf{x}, \mathbf{x_s}, \mathbf{p}, \omega)$ given by

$$\varphi(x_i, x_{s_i}, p_i, \omega) = \begin{cases} \exp(\mathrm{i}\omega p_i(x_{s_i} - x_{0_i})) & p_i \geq 0 \\ \exp(\mathrm{i}\omega p_i(x_{s_i} - x_{\max_i})) & p_i < 0 \end{cases}, \tag{6}$$

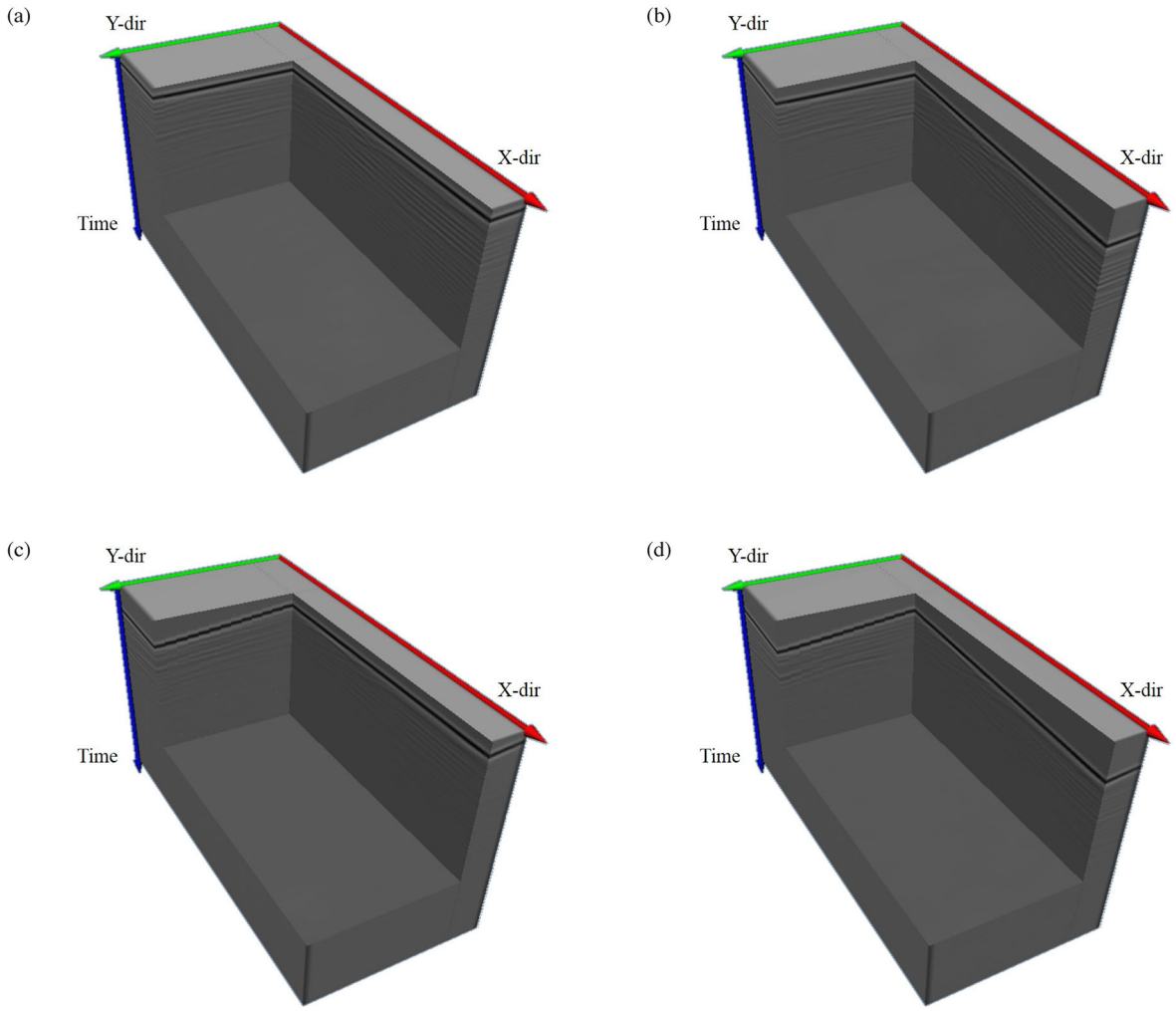

Figure 3. The time domain plane-wave gathers when (a) $p_x = 0$; $p_y = 0$, (b) $p_x = 0.08$; $p_y = 0$, (c) $p_x = 0$; $p_y = 0.08$ and (d) $p_x = 0.08$; $p_y = 0.08$.

Table 1. Comparison of the amount of data between the shot and plane-wave domains.

	Shot domain	Plane-wave domain
The number of data	$Ns \times Nr$	$Np \times Nr$

where x_{0_i} and $x_{\max_i}$ are the plane-wave origins when p_i are positive and negative, respectively. Plane-wave simulation in time domain may require extra propagation time due to delayed time, therefore, this is another cost implication. However, this problem can be avoidable in frequency domain because a phase shift in frequency domain substitutes for a time delay in time domain.

We solved eq. (5) with a direct solver that is accurate and efficient for a multisource problem. The direct solver only required back substitution to multisource vectors after once solving eq. (5). In this study, the Parallel Direct Sparse Solver (PARDISO), provided by the Intel Math Kernel Library (MKL), based on Lower Upper (LU) decomposition (Joo *et al.* 2012) was used. In the plane-wave domain approach, as the number of source vectors equals the number of ray parameters, which is generally much smaller than the number of sources, the number of back substitutions was also remarkably reduced.

CONDITIONS FOR THE GENERATION OF PLANE-WAVE DATA

When composing plane-wave data, we should select a suitable shot interval to avoid artefacts associated with large shot intervals. The condition for the shot interval is as follows:

$$\Delta s \leq \frac{1}{2 f_{\max} p_{\max}}, \tag{7}$$

where Δs is the shot interval, and $f_{\max}$ is the maximum frequency. In eq. (7), $p_{\max}$ should also be selected at a large enough value to properly image steep dips in the target area (Vigh & Starr 2008).

Cross-term artefacts occur due to cross correlation of different source wavefields when using a simultaneous source method. These cross-term artefacts can be reduced by selecting sufficient ray parameters, which is the plane-wave encoding strategy (Tao & Sen 2013). Zhang *et al.* (2005) suggested that the number of p should be approximately

$$N_p \geq \frac{W f_{\max}(\sin\theta_2 - \sin\theta_1)}{v_s}, \tag{8}$$

where v_s is the velocity at the surface shot location, W is the length of a common-receiver gather and θ is the take-off

angle (relative to the vertical) of the line source, with a range of $\theta_1 \le \theta \le \theta_2$.

INVERSION METHOD

FWI is based on minimization of the data residual between observed data ($\mathbf{d}_{\rm obs}$) and calculated data ($\mathbf{d}_{\rm cal}$). In our algorithm, these data sets are both plane-wave data, where $\mathbf{d}_{\rm obs}$ is transformed from recorded shot-gather data and $\mathbf{d}_{\rm cal}$ is generated by frequency-domain modelling using plane-wave data. The common misfit function consists of the L_2-norm of the residuals, and we employed the Gauss–Newton (GN) method, including regularization term, which is used for stabilizing the system and incorporating prior information (Tarantola 1987). The regularized misfit function of the GN method can be written as (Tarantola 1984; Pratt *et al.* 1998; Virieux & Operto 2009)

$$\begin{aligned}\mathbf{E}(\mathbf{m}) &= \mathbf{E}_d(\mathbf{m}) + \lambda \mathbf{E}_m(\mathbf{m}) \\ &= \frac{1}{2}\Delta\mathbf{d}^T\mathbf{W}_d\Delta\mathbf{d} + \lambda\frac{1}{2}\Delta\mathbf{m}^T\mathbf{C}^T\mathbf{C}\Delta\mathbf{m},\end{aligned} \tag{9}$$

where $\Delta\mathbf{d}$ is the data residual, $\Delta\mathbf{d}^T$ is the transpose of the data residual, $\Delta\mathbf{m}$ is model misfit, $\Delta\mathbf{m}^T$ is the transpose of the model misfit, $\mathbf{W}_d$ is data weighting operator and $\mathbf{C}$ is a roughness matrix. If $\mathbf{C}$ is replaced with the identity matrix $\mathbf{I}$, we call it a damped least-squares method (Levenberg 1944; Marquardt 1963). λ is a Lagrange multiplier, which is a damping factor to control the relative weight for the misfit functions in the data and model spaces.

The regularized Gauss–Newton solution that minimizes the above misfit function is as follows:

$$\Delta\mathbf{m} = \left[\mathbf{J}^T\mathbf{W}_d\mathbf{J} + \lambda\mathbf{C}^T\mathbf{C}\right]^{-1}\mathbf{J}^T\mathbf{W}_d\Delta\mathbf{d}, \tag{10}$$

where $\mathbf{J}$ is sensitivity, or the Jacobian matrix, the partial derivative of the wavefield with respect to each model parameter. In this study, we use the virtual source method and reciprocity concept suggested by Shin *et al.* (2001) to calculate the Jacobian matrix efficiently. In the plane-wave domain approach, this Jacobian matrix size decreases because of the reduction in data. Consequently, we can improve the efficiency of the memory in computing the inverse matrix.

We sum all Jacobian matrices calculated for each frequency because we carry out simultaneous multifrequency inversion using all selected frequencies at the same time. In this approach, the Jacobian may be predominantly influenced by the high-frequency component if a weighting factor is not applied for frequencies. To prevent this, we employed the multifrequency data weighting proposed by Hu *et al.* (2009); the weighting factor was as follows:

$$\mathrm{W}_{d,k} = \left(\frac{\frac{1}{\omega_k^2}}{\sum_{i=1}^{nfreq}\frac{1}{\omega_i^2}}\right)^2, \tag{11}$$

where $W_{d,k}$ is the kth multifrequency data weighting, and *nfreq* is the frequency number used in the inversion. This weighting factor balances the influence of the frequency components on the Jacobian.

In inversion, it is difficult to determine a suitable value for the damping factor to achieve stability while also preserving resolution, as λ is usually chosen by trial and error to yield a solution that has a reasonably small prediction error (Menke 1984). Yi *et al.* (2003) suggested active constraint balancing (ACB), a method to determine the spatially varying Lagrangian multipliers $\lambda(x_i, y_i, z_i)$ using a spread function for the dc resistivity inversion problem to easily acquire a suitable damping factor satisfactory for both stability and resolution. However, because the resolution of seismic data shows different characteristics in comparison with dc resistivity data due to a different governing equation, Joo *et al.* (2012) modified the ACB scheme to apply it to FWI through alteration of the spread function. In this study, we adopt Joo *et al.*'s ACB method in our inversion to determine an optimum $\lambda(x_i, y_i, z_i)$, which varies spatially according to sensitivities.

In the inversion process, the updated model parameters are sometimes beyond the range of physically meaningful values. Kim *et al.* (1999) suggested an inequality constraint to prevent this problem. We assumed that model parameters are known as

$$a < m_i < b, \quad i = 1, 2, \ldots, k. \tag{12}$$

The parameter is bounded by a and b, which are physically meaningful. We defined a new parameter x as follows:

$$x_i = \ln\left(\frac{m_i - a}{b - m_i}\right). \tag{13}$$

The perturbation of x_i is given by

$$\delta x_i = \frac{b - a}{(m_i - a)(b - m_i)}\delta m_i. \tag{14}$$

Thus, updated model parameters were renewed as

$$m_{i+1} = \frac{a(b - m_i) + b(m_i - a)\,\mathrm{e}^{\delta x_i}}{(b - m_i) + (m_i - a)\,\mathrm{e}^{\delta x_i}}. \tag{15}$$

We first obtained δx of eq. (14) in the inversion and then calculated the real updated model parameter using eq. (15).

SOURCE NORMALIZATION METHOD

Estimation of the source wavelet is very important to successfully implement the FWI; therefore, most FWI algorithms have a source-estimation process. However, this is not necessary in our algorithm because we applied a source-normalization technique to our FWI algorithm. Source normalization is a method to remove the effect of source in an inversion through normalization of the wavefield by the data from a reference receiver.

Lee & Kim (2003) defined the normalized wavefield in the frequency domain as follows:

$$t_{ji}^d(\omega) = \frac{d_{ji}^d(\omega)}{d_{1i}^d(\omega)} = \frac{p_{ji}^d(\omega)s_i(\omega)}{p_{1i}^d(\omega)s_i(\omega)} = \frac{p_{ji}^d(\omega)}{p_{1i}^d(\omega)}, \tag{16}$$

where d_{ji}^d and p_{ji}^d are the observed data and the impulse response at the jth receiver position attributable to a source $s_i(\omega)$ at the ith source position, respectively. d_{1i}^d and p_{1i}^d are the observed data and the impulse response at a reference receiver, respectively. The normalized wavefields are calculated at the receiver positions ($j = 2, 3, \ldots, Nr$) except for the reference receiver ($j = 1$), and the normalized wavefield is the same as the normalized impulse response of the medium.

Lee & Kim (2003) applied this approach to shot gathers from point sources, and different shot gathers have been individually normalized by different reference data. However, since we used plane-wave gathers that were obtained by using all sources simultaneously, i in eq. (16) is not a source number but a ray parameter. Thus, different plane-wave gathers with different ray parameters should be individually normalized by different reference data.

To incorporate this source-normalization scheme into our FWI, we investigated the influence of the reference data on our inversion result. For point source data, data from the nearest receiver

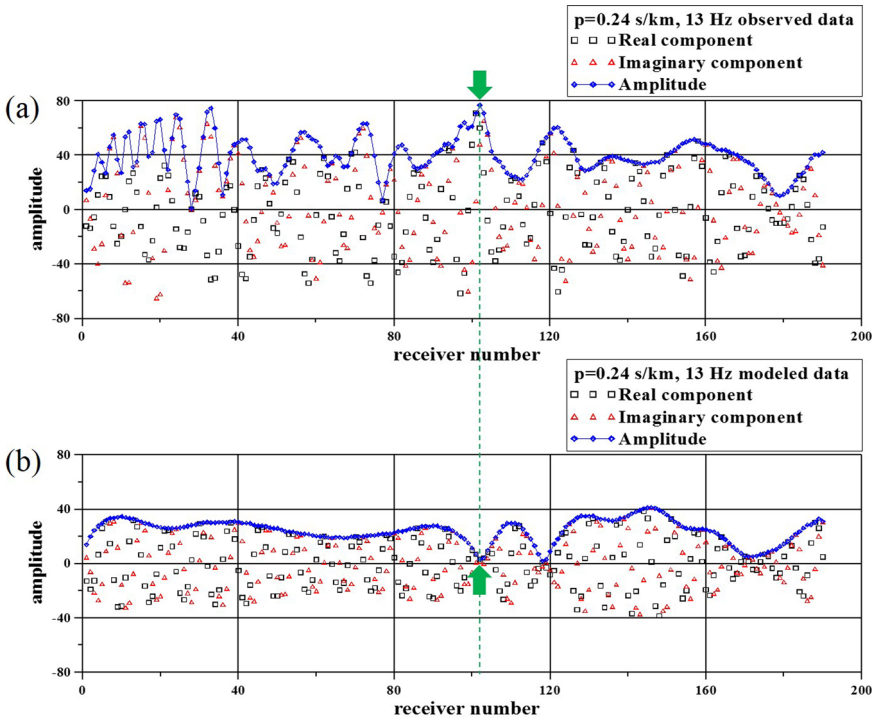

Figure 4. (a) The observed and (b) modelled plane-wave data in frequency domain at 13 Hz ($p = 0.24$ s km^{-1}). Green arrows and the dashed line indicate the selected point that corresponds to a reference data set at receiver number 102.

to the source location are usually selected (Lee & Kim 2003; Joo *et al.* 2012). This selected receiver is not near a zero crossing point because data at the location closest to the source have the highest amplitude in both observed and modelled data. However, in the case of plane-wave data, it is possible to select an almost zero crossing point in modelled data if we select the point of highest amplitude in observed data. Fig. 4 shows an example of this; (a) and (b) are the observed data and the modelled data for the initial model in frequency domain at 13 Hz ($p = 0.24$ s km^{-1}), respectively. The green arrows indicate the reference data at the selected receiver location in the observed and modelled data. The highest amplitude point in the observed data corresponds to the almost zero crossing point in the modelled data. These near-zero crossing data can make a normalized field unstable. To make the normalized wavefield stable, we developed a method to automatically reselect a different point when the selected reference point has a value with very low amplitude.

NUMERICAL EXPERIMENTS

Verification of the plane-wave inversion scheme

We generated 2-D synthetic data for the velocity model shown in Fig. 5, which is modified from the original SEG/EAGE overthrust model. The original model consists of 801 × 187 grid cells in 2-D section with 25-m-horizontal and vertical grid intervals. However, because we used 15-m-grid intervals to prevent dispersion during propagation, we modified the model of grid cells to 1602 × 374, which is double the extension of the original grid, to compensate for the lower resolution due to the 15-m-grid interval. Implementing the conventional FWI and our FWI using these generated synthetic data, we compared the two methods to determine the efficiency of our algorithm. Fig. 6 is the initial model used in the FWI. This model is used in all of the following 2-D examples. We selected six frequencies ranging from 3 to 15 Hz for the inversion and employed simultaneous multifrequency inversion using all selected frequencies. In the FWI with the plane-wave approach, 41 ray parameters and 390 receivers were used, whereas 391 sources and 390 receivers were used in the FWI with the shot domain approach. For this model, 41 ray parameters were enough to satisfy the condition of plane-wave encoding described in the previous section. Thus, the inversion was efficiently performed using only about a tenth the amount of data, and the run time of the FWI with plane-wave domain was approximately 12 times faster than that with shot domain (Table 2). Fig. 7 shows the inverted results with the plane-wave and shot domain approaches, respectively. Both are comparable to the true model.

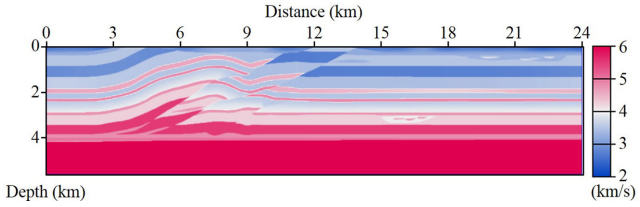

Figure 5. The velocity model modified from the original SEG/EAGE overthrust model.

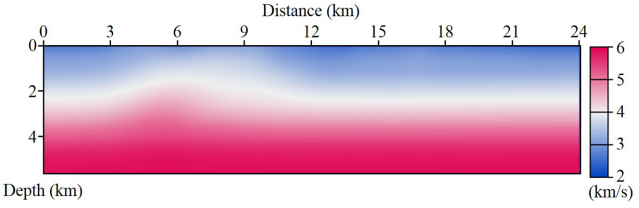

Figure 6. Initial model used in FWI.

Table 2. Comparison of the computational efficiency between shot and plane-wave domain approaches.

	The number of data	Memory cost	Run time per iteration
Plane-wave domain	41 × 390 × 6	1	1
Shot domain	391 × 391 × 6	9.5	12.7

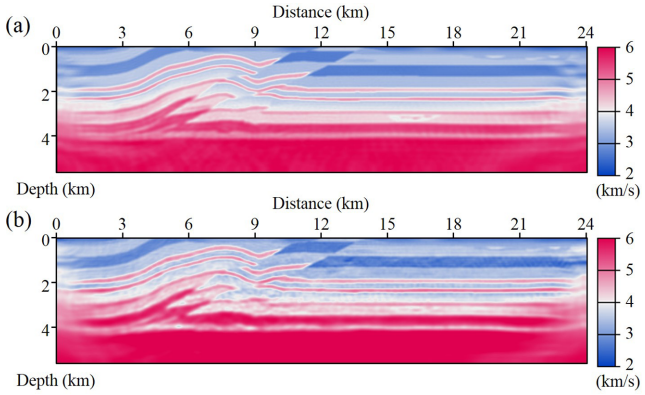

Figure 7. The inverted model at the 20th iteration with (a) the plane-wave domain approach and (b) the shot domain approach.

Next, we carried out FWI with only 196 receivers, which is half the number of receivers used in the first test. Except for the amount of data, which differed due to the reduction in receivers, the same parameters were used in this inversion as in the first test. The inverted result for the plane-wave domain was still comparable to the result using all receivers, whereas the inverted result with shot domain was worse than that using all receivers (Fig. 8). Additionally, the rms error stably converged to the low level, whereas that from the shot domain approach showed unstable features (Fig. 9). Furthermore, we can confirm that the velocity profiles of the inverted results with the plane-wave domain are almost exact, despite using only 196 receivers (Fig. 10).

Source normalization and noise tests

To investigate the performance of the normalized wavefield, we chose a reference source wavelet with 6 Hz main frequency. The source wavelets used in modelling had 5 per cent random variations in phase and amplitude from this reference source wavelet (Fig. 11). This variation simulates the real field situation in that each source

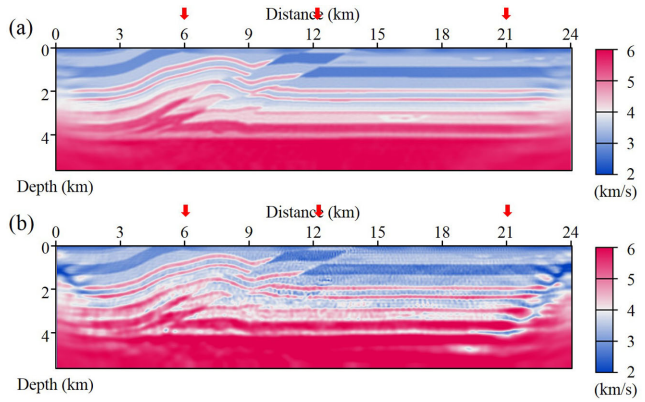

Figure 8. The inverted result with only half the number of receivers used in the previous test. The inverted model at the 20th iteration with (a) the plane-wave domain approach and (b) the shot domain approach.

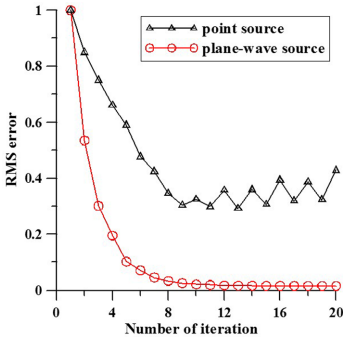

Figure 9. Rms curves for the inversions with the shot domain approach (black line) and the plane-wave domain approach (red line).

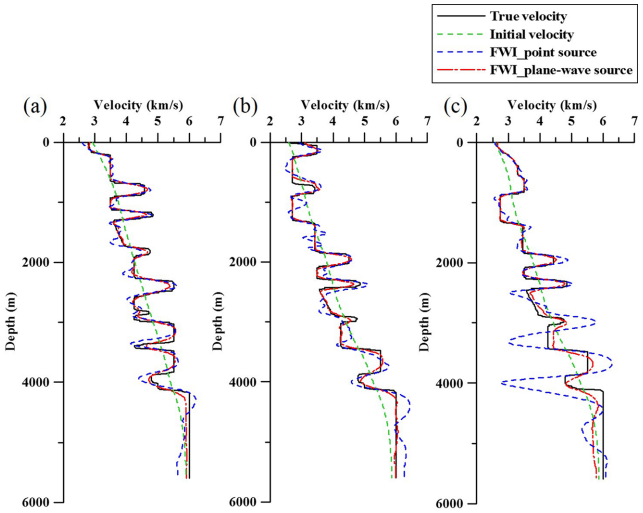

Figure 10. The vertical velocity profiles of the true model, initial model, and inverted models with the shot domain and plane-wave domain approach at (a) $x = 6$ km, (b) $x = 12.3$ km and (c) $x = 21$ km indicated by red arrows in Fig. 7.

has slightly different amplitudes and phase characteristics in field application. As shown in Fig. 12, the inverted model with the source-normalization scheme was approximate to the true model, whereas that without it had noise artefacts. Furthermore, because of the effect of randomly varied sources, the rms error of the inversion without the source-normalization scheme increased after 10 iterations, as shown in Fig. 13.

Random noise can greatly affect the result of FWI, and it can often make the inversion fail. Therefore, it is important to test how the FWI algorithm works for data with random noise. We

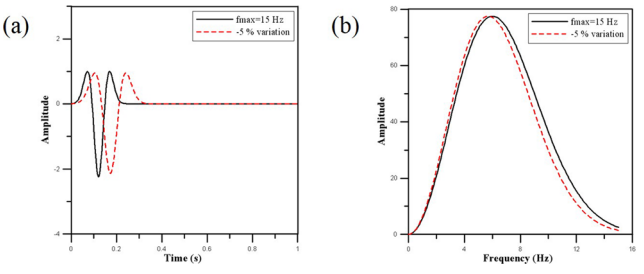

Figure 11. (a) The source wavelets and (b) their frequency spectra. Black solid lines correspond to the reference source, and red dashed lines correspond to the source example, with −5 per cent variation in phase and amplitude of the reference source.

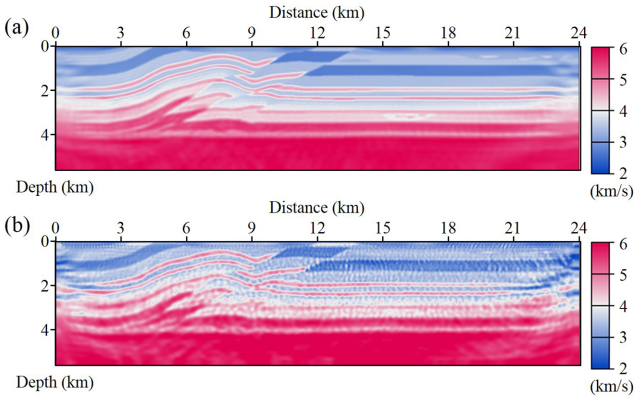

Figure 12. (a) The inverted model at the 20th iteration with source normalization and (b) the inverted model at the 10th iteration without source normalization.

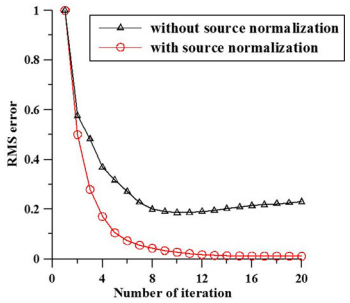

Figure 13. Rms curves for the inversions with (red line) and without (black line) source normalization.

applied our inversion algorithm to the noise-added data set with 391 sources and 196 receivers. The SNR of shot gather with random noise was 3.25 (Fig. 14). We carried out FWI with plane-wave data that were transformed from these noisy data (Fig. 14b). Although considerable random noise was added to the data, the inversion was performed successfully, as shown in Fig. 15.

Application to 3-D overthrust model

Finally, we applied the plane-wave method to the 3-D synthetic data obtained from part of the 3-D SEG/EAGE overthrust model to verify the validity of our algorithm for 3-D data. The finite elements were 300 × 100 × 150 elements, with each element 25 × 25 × 15 m to avoid dispersion; therefore the dimensions of the model (Fig. 16a)

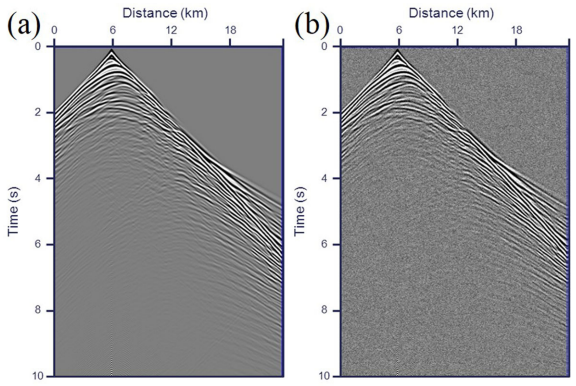

Figure 14. (a) The noise-free shot gather and (b) the noise-added shot gather (SNR = 3.25).

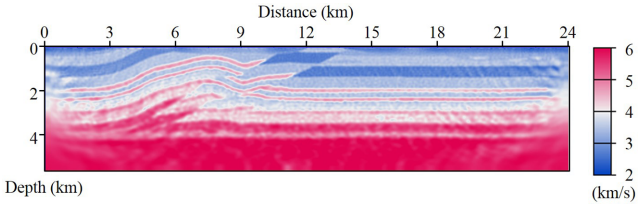

Figure 15. The inverted model with the plane-wave approach using random noise-added data. The number of receivers used in the inversion was 196.

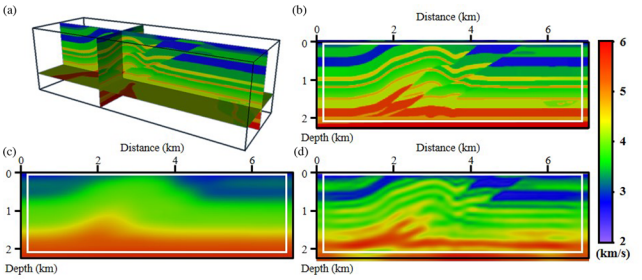

Figure 16. (a) 3-D representation of the overthrust model and vertical slices through the middle of the (b) true, (c) initial and (d) inverted models. The white boxes indicate the inversion area.

were 7.5 × 2.5 × 2.25 km. We generated synthetic data with 138 × 38 (5244) sources and 69 × 10 (690) receivers, but only 123 plane-wave gathers were used in the inversion. Because the length of the *y*-axis is much shorter than that of the *x*-axis and the dip of structure in the *y*-axis is not as steep as that in the *x*-axis, we can use fewer ray parameters in the *y*-axis than in the *x*-axis. We used five frequencies ranging from 4 to 10 Hz in the inversion. Fig. 16 shows the true, starting, and inverted model of the vertical section in the middle of the model. Fig. 17 displays the depth slices of the inverted model at 300 and 750 m. The white boxes in Figs 16 and 17 indicate practical inverted areas except PML boundary regions. The inversion result shown in Fig. 16(a) has a low resolution compared with those of 2-D examples because we used lower frequencies and a lower resolution model (about $\frac{1}{2}$) than the one in the 2-D examples in order to handle the 3-D model efficiently. However, even though the overthrust model used had a complex structure including thin layers and relatively low resolution, our inversion results overall described not only overthrust structures as targets but also thin layers (Fig. 16). Therefore, we can identify the existence and shape of the narrow channels shown in depth slices (Fig. 17).

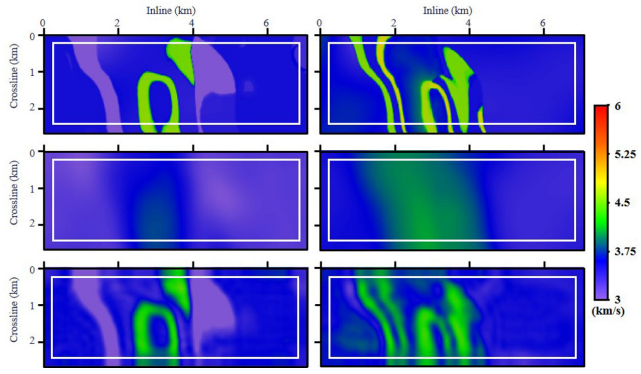

Figure 17. Horizontal slices at 300 (left-hand panels) and 750-m (right-hand panels) depths of the true (top panels), initial (middle panels) and inverted (bottom panels) models. The white boxes indicate the inversion area.

CONCLUSIONS

We have developed an efficient simultaneous-source 3-D FWI scheme using plane-wave encoding in the frequency domain. As the number of plane-wave gathers is far fewer than that of the original acquired data, we could significantly reduce the computational cost for the inversion. For the 2-D modified SEG/EAGE overthrust model, the amount of memory and run time per iteration could be reduced to about one-tenth by using the plane-wave domain approach compared with the shot domain approach. Additionally, our source-normalization scheme successfully worked for the data obtained from randomly varied sources with 5 per cent variation from the reference source wavelet. The inverted result showed an almost identical image to the true model without any noisy artefacts due to source variation. Furthermore, our plane-wave domain approach successfully inverted noise-added data even though the SNR was a relatively high value (SNR = 3.25). By applying the proposed FWI to a complex 3-D overthrust model including complex channels, we obtained a reasonable reconstructed velocity model. Overthrust structures with thin layers were well depicted in the vertical slice, and the shape and location of channels were sufficiently exposed in the depth slices.

ACKNOWLEDGEMENTS

This work was supported by the Human Resources Development program (No. 20134010200520) of the Korea Institute of Energy Technology Evaluation and Planning (KETEP) grant funded by the Korea government Ministry of Trade, Industry and Energy.

REFERENCES

Ben-Hadj-Ali, H., Operto, S. & Virieux, J., 2011. An efficient frequency-domain full waveform inversion method using simultaneous encoded sources, *Geophysics,* **76**(4), R109–R124.

Boonyasiriwat, C. & Schuster, G.T., 2010. 3D multisource full-waveform inversion using dynamic random phase encoding, in *Proceedings of the 80th Annual International Meeting,* SEG, Expanded Abstracts, 29, 1044–1049.

Dai, W. & Schuster, G.T., 2013. Plane-wave least-squares reverse-time migration, *Geophysics,* **78**(4), S165–S177.

Guitton, A. & Díaz, E., 2012. Attenuating crosstalk noise with simultaneous source full waveform inversion, *Geophys. Prospect.,* **60,** 759–768.

Hu, W., Abubakar, A. & Habashy, T.M., 2009. Simultaneous multifrequency inversion of full-waveform seismic data, *Geophysics,* **74,** R1–R14.

Joo, Y., Seol, S.J. & Byun, J., 2012. Acoustic full-waveform inversion of surface seismic data using the Gauss-Newton method with active constraint balancing, *Geophys. Prospect.,* **61,** 166–182.

Kim, H.J., Song, Y. & Lee, K.H., 1999. Inequality constraint in leastsquares inversion of geophysical data, *Earth Planets Space,* **51,** 255–259.

Krebs, J.R., Anderson, J.E., Hinkley, D., Neelamani, R., Lee, S., Baumstein, A. & Lacasse, M.D., 2009. Fast full-wavefield seismic inversion using encoded sources, *Geophysics,* **74**(6), WCC177–WCC188.

Lee, L.H. & Kim, H.J., 2003. Source-independent full-waveform inversion of seismic data, *Geophysics,* **68,** 2010–2015.

Levenberg, K., 1944. A method for the solution of certain non-linear problems in least squares, *Quarter. Appl. Math.,* **2,** 164–168.

Liu, F., Hanson, D.W., Whitmore, N.D., Day, R.S. & Stolt, R.H., 2006. Toward a unified analysis for source plane-wave migration, *Geophysics,* **71**(4), S129–S139.

Marfurt, K.J., 1984. Accuracy of finite-difference and finite-element modeling of the scalar and elastic wave equations, *Geophysics,* **49,** 533–549.

Marquardt, D.W., 1963. An algorithm for least-squares estimation of nonlinear parameters, *J. Soc. Ind. Appl. Math.,* **11,** 431–441.

Menke, W., 1984. *Geophysical Data Analysis: Discrete Inverse Theory,* Academic Press Inc.

Operto, S., Virieux, J., Amestoy, P., L'Excellent, J., Giraud, L. & Ali, H.B.H., 2007. 3D finite-difference frequency-domain modeling of viscoacoustic wave propagation using a massively parallel direct solver: a feasibility study, *Geophysics,* **72**(5), SM195–SM211.

Pratt, R.G., 1999. Seismic waveform inversion in the frequency domain. Part 1: theory and verification in a physical scale model, *Geophysics,* **64,** 888–901.

Pratt, R.G., Shin, C. & Hicks, G.J., 1998. Gauss-Newton and full Newton methods in frequency-space seismic waveform inversion, *Geophys. J. Int.,* **133,** 341–362.

Romero, L.A., Ghiglia, D.C., Ober, C.C. & Morton, S.A., 2000. Phase encoding of shot records in prestack migration, *Geophysics,* **65,** 426–436.

Shin, C. & Min, D., 2006. Waveform inversion using a logarithmic wavefield, *Geophysics,* **71**(3), R31–R42.

Shin, C., Yoon, K., Marfurt, K.J., Park, K., Yang, D., Lim, H.Y., Chung, S. & Shin, S., 2001. Efficient calculation of a partial-derivative wavefield using reciprocity for seismic imaging and inversion, *Geophysics,* **66**(6), 1856–1863.

Stoffa, P.L., Sen, M.K., Seifoullaev, R., Pestana, R. & Fokkema, J., 2006. Plane-wave depth migration, *Geophysics,* **71**(6), S261–S272.

Tao, Y. & Sen, M., 2013. Frequency-domain full waveform inversion with plane-wave data, *Geophysics,* **78**(1), P.R13–R23.

Tarantola, A., 1984. Inversion of seismic reflection data in the acoustic approximation, *Geophysics,* **49,** 1259–1266.

Tarantola, A., 1987. *Inverse Problem Theory: Methods for Data Fitting and Parameter Estimation,* Elsevier Science Publishers.

Vigh, D. & Starr, E.W., 2008. 3D prestack plane-wave, full-waveform inversion, *Geophysics,* **73**(5), VE135–VE144.

Virieux, J. & Operto, S., 2009. An overview of full waveform inversion in exploration geophysics, *Geophysics,* **74**(6), WCC1–WCC26.

Whitmore, N., 1995. An imaging hierarchy for common angle plane wave seismograms, *PhD thesis,* University of Tulsa.

Yi, M.J., Kim, J.H. & Chung, S.H., 2003. Enhancing the resolving power of least-squares inversion with active constraint balancing, *Geophysics,* **68,** 931–941.

Zhang, Y., Sun, J., Notfors, C., Gray, S.H., Chernis, L. & Young, J., 2005. Delayed-shot 3D depth migration, *Geophysics,* **70**(5), E21–E28.